Progress In Electromagnetics Research, PIER 58, 1–19, 2006

ELECTROMAGNETIC RADIATION FROM MOVING FRACTAL SOURCES: A PLANE-WAVE SPECTRAL APPROACH

W. Arrighetti, P. De Cupis, and G. Gerosa

Electronic Engineering Department
Università degli Studi di Roma "La Sapienza"
via Eudossiana 18, 00184, Rome, Italy

Abstract—In this work the solution to the problem of electromagnetic radiation from (pre-)fractal antennas is performed by means of Plane-Wave field representation based on closed-form Fourier transforms of the self-similar current patterns. The generalization to the case of uniformly translating antennas is then accomplished through the Frame-Hopping Method by exploiting special-relativistic covariance properties of Plane-Wave spectra.

1. INTRODUCTION

Many fractal sets are built through the application of an Iterated Function System (IFS), i.e., by applying a suitable contraction sequence to a starting set; by iterating such application N times the N^{th} order prefractal set is obtained, whereas the fractal set at the limit $N \to \infty$ is reached. Such iterative generation scheme produces self-similar sets, whose geometrical features are replicated at various (even infinite) decreasing scales. When establishing a theoretical approach to physical problems on (pre-)fractal lattices that are generated by IFSs, it is important to express the intrinsic iterative nature in terms of the involved mathematical operators in order to highlight solutions' self-similarity and to explicit efficient recursive procedures for describing space-time distributions of the physical quantities at every iteration's increment $N \to N + 1$.

(Pre-)fractal geometries have been recently pioneered in electromagnetic (EM) applications, especially for developing high-performance multi-band antennas [1–6] and resonators [7, 8]; in fact, the multi-scale self-similarity properties of the radiating structure involve a substantial 'invariance' of the emitted field features with respect to the wave-length.

In this paper a spectral-domain approach for the theoretical study of radiation by fractal shaped antennas is presented; radiating geometries whose generating IFS is based on affinities (i.e., translations, rotations and dilations) are considered. Since this kind of spatial transformations have simple analytical counterparts in the Fourier domain, it is possible to establish an efficient iterative procedure for a closed-form spectral description of the source current distribution. For the same reasons the spectral properties of a self-similar resonator bears enough information to compute the fractal dimension of the cavity [8]. Then the evaluation of the EM field radiated by the antenna is directly accomplished by integral-expanding the Plane-Wave (PW) radiations originated by the various spectral components of the source current. In this way we avoid direct space-domain integral-differential computation on the fractal structure (e.g., convolution between tensor Green function and currents), which involves some 'critical' theoretical issues (e.g., tangent vectors cannot be properly defined in classical way almost anywhere on the fractal [9]).

Moreover, the resulting PW representation of the emitted EM field admits an analytically-simple generalization to the case of moving antennas (i.e., in the presence of relative motion, e.g., uniform translation, between the current source lattice and the EM field observer); this is fundamental in order to establish a theoretical framework for the development of fractal-shaped devices to be specifically employed in mobile telecommunication systems. In fact, the special-relativistic extension is based on a two-step Frame Hopping method [10, 11], i.e., the solution is at first evaluated in the reference frame where the signal transmitter appears at rest (co-moving frame) through the customary motionless technique and, secondly, the Field Relativistic Covariance Transformation (FRCT) is applied to the radiated EM field in order to compute its expression in the reference frame where the signal receiver appears at rest; the analytic effort involved by the FRCT would be cumbersome for a generic expression of the EM field, but in our case it is minimized since the EM field is represented in terms of a PW spectrum, resulting in a mere application of manageable alteration formulas for the PW parameters (frequency, propagation unit vector, amplitude) relevant to the various spectral components implicated in the integral expansion [12, 13] (see also [14–16] about the application of the PW spectral representation for relativistic scattering).

2. FOURIER TRANSFORM OF ITERATED FUNCTION SYSTEMS

Let $\{\mathbf{w}_1, \mathbf{w}_2, \ldots, \mathbf{w}_p\}$ be an IFS defined in $\mathbb{R}^d$ (see Appendix for mathematical background), i.e., each contraction mapping $\mathbf{w}_j : \mathbb{R}^d \to \mathbb{R}^d$ is defined by d equations like $\mathbf{y} = \mathbf{w}_j(\mathbf{x})$:

$$\begin{cases} y_1 = w_{j,1}(x_1, x_2, \ldots, x_d) \\ y_2 = w_{j,2}(x_1, x_2, \ldots, x_d) \\ \qquad\vdots \\ y_d = w_{j,d}(x_1, x_2, \ldots, x_d) \end{cases}, \quad \begin{array}{c} ||\mathbf{w}_j(\mathbf{x}) - \mathbf{w}_j(\mathbf{x}')|| \leq c_j||\mathbf{x} - \mathbf{x}'||, \\ \forall \mathbf{x},\, \mathbf{x}' \in \mathbb{R}^d. \end{array} \tag{1}$$

The application of an IFS to a set in the Euclidean space can be thought as mapping of the IFS to the characteristic function[1] of the set $\chi_E(\mathbf{x})$; its Fourier transform indicated as $\breve{\chi}_E(\boldsymbol{\kappa}) := \int e^{i\boldsymbol{\kappa}\cdot\mathbf{x}}\chi_E(\mathbf{x})d\mathbf{x}$ ($i = \sqrt{-1}$). When the set is the N^{th} prefractal $E_N = \mathbf{w}^N(E)$ under the given contraction mapping of a 'just-touching' IFS

$$\mathbf{w}(E) := \bigcup_{j=1}^{p} \mathbf{w}_j(E), \tag{2}$$

and especially if $\{\mathbf{w}_1, \mathbf{w}_2, \ldots, \mathbf{w}_p\}$ are similarities, elementary Fourier-transform properties can be applied to the magnification, reflection and/or translation of the characteristic function for closed-form computing purposes.

Suppose $\mathbf{w}_j(\mathbf{x}) = \alpha_j\mathbf{x} + \mathbf{t}_j$, where $\alpha_j \in \mathbb{R}^*$ and $\mathbf{t}_j \in \mathbb{R}^d$, which is a quite general form of affinity mapping; then:

$$\begin{aligned} \breve{\chi}_{\mathbf{w}(E)}(\boldsymbol{\kappa}) = \int_{\mathbb{R}^d} e^{i\boldsymbol{\kappa}\cdot\mathbf{x}}\chi_{\mathbf{w}(E)}(\mathbf{x})\mathrm{d}x &= \sum_{j=1}^{p} \int_{\mathbb{R}^d} e^{i\boldsymbol{\kappa}\cdot\mathbf{x}}\chi_E(\alpha_j\mathbf{x} + \mathbf{t}_j)\mathrm{d}x \\ &= \sum_{j=1}^{p} e^{-i\boldsymbol{\kappa}\cdot\mathbf{t}_j}\alpha_j^{-1}\breve{\chi}_E(\alpha_j^{-1}\boldsymbol{\kappa}) \end{aligned} \tag{3}$$

This formula allows us the computation or the spectral Fourier Transform of $\mathbf{w}^{N+1}(E)$ as depending on $\mathbf{w}^N(E)$'s one:

$$\breve{\chi}_{\breve{S}_{d,\,N+1}}(\boldsymbol{\kappa}) = \sum_{j=1}^{p} e^{-i\boldsymbol{\kappa}\cdot\mathbf{t}_j}\alpha_j^{-1}\breve{\chi}_{\breve{S}_{d,\,N+1}}(\alpha_j^{-1}\boldsymbol{\kappa}). \tag{4}$$

1 The characteristic function $\chi_E : E \to \{0, 1\}$ is defined as follows: $\chi_E(x) = 1$ if $x \in E$, otherwise $\chi_E(x) = 0$ if $x \notin E$.

For instance, let $\chi_{\check{S}_{d,\,N}}(x)$ be the characteristic function of the d-dimensional Sierpinski sponge's N^{th} prefractal $\check{S}_{d,\,N}$ which, for $d = 2$ and $N \to \infty$ coincides with the well-known Sierpinski carpet $\check{S}_2$. The characteristic functions of the Sierpinski sponge prefractals can be represented as the following finite sums of rectangular pulses [18, 19]:

$$\chi_{\check{S}_{d,\,N}}(\mathbf{x}) = \mathrm{rect}_{\mathbf{1}_d}\mathbf{x} - \sum_{h=1}^{N} \sum_{\mathbf{c}_h \in \Lambda_h^d \cap \check{S}_{d,\,h-1}} \mathrm{rect}_{3^{-h}\mathbf{1}_d}(\mathbf{x} - \mathbf{c}_h), \qquad \begin{cases} \Lambda_h = \Lambda_h^+ \cup \Lambda_h^- \\ \Lambda_h^{\pm} = \left\{ \dfrac{1 \pm 2n}{2 \cdot 3^h} \right\}_{n \in \mathbb{N}} \end{cases}, \tag{5}$$

where $L_{d,\,h}$ is the set of even integer d-plets divided by $2{\cdot}3^h$. A recursion scheme can be extracted to compute the $(N+1)^{\text{th}}$ prefractal's spectral and characteristic functions from the N^{th} prefractal ones:

$$\begin{aligned} \chi_{\check{S}_{d,\,N+1}}(\mathbf{x}) &= \sum_{\mathbf{h} \in M_d} \chi_{\check{S}_{d,\,N}}(3(\mathbf{x} + \mathbf{h})) \;\Leftrightarrow \\ \breve{\chi}_{\check{S}_{d,\,N+1}}(\boldsymbol{\kappa}) &= \frac{1}{3}\breve{\chi}_{\check{S}_{d,\,N}}(3^{-1}\boldsymbol{\kappa}) \sum_{\mathbf{h} \in M_d} e^{-i\mathbf{h}\cdot\boldsymbol{\kappa}}, \end{aligned} \tag{6}$$

with $M_d = \{-\frac{1}{2},\, 0,\, \frac{1}{2}\}^d \setminus \{\mathbf{0}_d\}$.

Considering the spectral duality between 'rect' and 'sinc' functions[2], the Fourier transform of Eq. (5) can be straightforwardly evaluated:

$$\begin{aligned} \breve{\chi}_{\check{S}_{d,\,N}}(\boldsymbol{\kappa}) &= \int_{\check{S}_{d,\,N}} e^{i\mathbf{x}\cdot\boldsymbol{\kappa}}\mathrm{d}x \equiv \int_{\mathbb{R}^N} e^{i\mathbf{x}\cdot\boldsymbol{\kappa}}\chi_{\check{S}_{d,\,N}}(\mathbf{x})\mathrm{d}x \\ &= \mathrm{sinc}\frac{\boldsymbol{\kappa}}{2} - \sum_{h=1}^{N} 3^{-nh}\mathrm{sinc}\left(\frac{\boldsymbol{\kappa}}{2 \cdot 3^h}\right) \cdot \sum_{\mathbf{c}_h \in \Lambda_h^d \cap \check{S}_{d,\,h-1}} e^{i\mathbf{c}_h\cdot\boldsymbol{\kappa}} \end{aligned} \tag{7}$$

By virtue of Cartesian symmetry with respect to $\mathbf{0}_d \in \mathbb{R}^d$ and applying

2 For $\mathbf{x} = (x_k)_{1 \le k \le d}$, d-dimensional 'rect' and 'sinc' functions are defined as $\mathrm{sinc}\mathbf{x} := \Pi_k \mathrm{sinc}x_k$ and $\mathrm{rect}_{\alpha\mathbf{1}_d}\mathbf{x} = \Pi_k \mathrm{rect}_\alpha x_k$, $\mathrm{rect}_\alpha x$ is the square pulse equal to 1 in $[-a,\, a]/2$ and 0 everywhere else. Also $\mathbf{1}_d = (1,\, 1, \ldots,\, 1)$ and $\mathbf{0}_d = (0,\, 0, \ldots,\, 0)$.

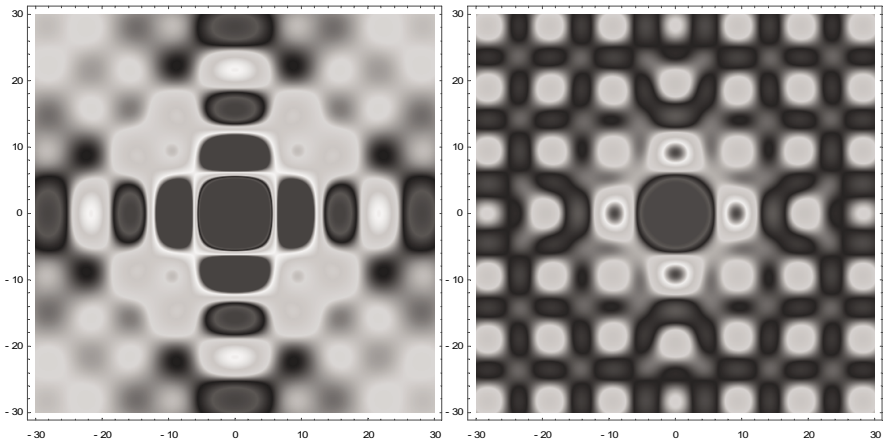

Figure 1. Spectral function of Sierpinski two-dimensional sponge's 1st and 2nd prefractal $\breve{\chi}_{\breve{S}_{2,\,n}}(\boldsymbol{\kappa})$, for $\boldsymbol{\kappa} \equiv (\kappa_1, \kappa_2) \in 30[-1, 1]^2$ (for $N = 1, 2$, respectively). Normalized grayscale for absolute value is used hereinafter.

elementary Euler's formulas, one gets:

$$\breve{\chi}_{\breve{S}_{d,\,N}}(\boldsymbol{\kappa}) = \operatorname{sinc}\frac{\boldsymbol{\kappa}}{2} - \frac{1}{3^d}\operatorname{sinc}\frac{\boldsymbol{\kappa}}{6} - 2\sum_{h=2}^{N} 3^{-dh}\operatorname{sinc}\left(\frac{\boldsymbol{\kappa}}{2\cdot 3^h}\right) \sum_{\mathbf{c}_h \in \Lambda_h^{+d} \cap \breve{S}_{d,\,h-1}} \cos(\mathbf{c}_h \cdot \boldsymbol{\kappa}), \quad (8)$$

Sample plots for Fourier transforms of the prefractal Sierpinski carpet's (2D) and sponge's (3D) characteristic functions are given in Fig. 1 and Fig. 2, respectively.

3. PLANE-WAVE SPECTRAL TECHNIQUES FOR RADIATION PROBLEMS

3.1. The Motionless Problem

For a EM radiation problem in vacuum, the EM field is solution of the following Maxwell equations:

$$\nabla \times \left\{ \begin{array}{c} \boldsymbol{E} \\ \boldsymbol{H} \end{array} \right\}_{\mathbf{r},\,t} = \frac{\partial}{\partial t} \left\{ \begin{array}{c} -\mu_0 \boldsymbol{H} \\ \varepsilon_0 \boldsymbol{E} \end{array} \right\}_{\mathbf{r},\,t} + \left\{ \begin{array}{c} \mathbf{0} \\ \boldsymbol{J} \end{array} \right\}_{\mathbf{r},\,t} \quad (9)$$

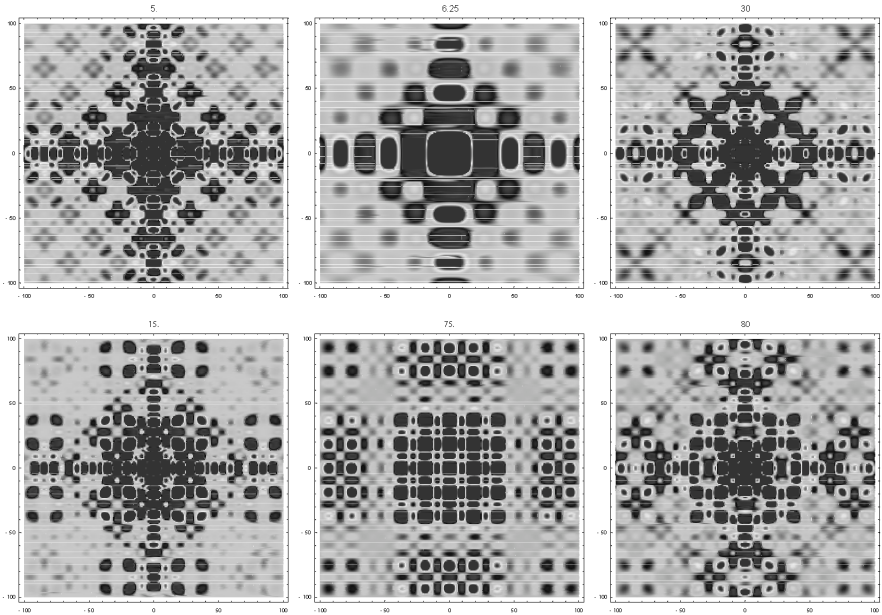

Figure 2. Slices of the Sierpinski three-dimensional sponge 3rd prefractal's spectral function $\breve{\chi}_{\breve{S}_{3,3}}(\boldsymbol{\kappa})$, for $\boldsymbol{\kappa} \equiv (\kappa_1, \kappa_2, \kappa_3) \in 100[-1, 1]^2 \times \{5, 6.25, 30, 15, 75, 80\}$.

where $\boldsymbol{E}$, $\boldsymbol{H}$, $\boldsymbol{J}$ are the electric field, the magnetic field and the electric current source distribution at position $\mathbf{r} = x_m \hat{\mathbf{x}}^m$ and time t relevant to the space-time reference system Σ, respectively; $\{\hat{\mathbf{x}}^m\}_{m=1,2,3}$ and $\{x_m\}_{m=1,2,3}$ are the Cartesian unit vectors and coordinates, respectively[3]; ∇ is the nabla operator with respect to the space coordinates in Σ; ε_0, μ_0 are the vacuum permettivity and permeability, respectively.

By introducing the following quadruple Fourier-transformation:

$$\left\{\breve{\mathbf{E}}, \breve{\mathbf{H}}, \breve{\mathbf{J}}\right\}_{\boldsymbol{\kappa},\omega} = \iiint_{\mathbb{R}^3} \mathrm{d}\mathbf{r} \int_{-\infty}^{+\infty} \left\{\boldsymbol{E}, \boldsymbol{H}, \boldsymbol{J}\right\}_{\mathbf{r},t} e^{i(\boldsymbol{\kappa}\cdot\mathbf{r}-\omega t)} \mathrm{d}t, \tag{10}$$

$$\left\{\boldsymbol{E}, \boldsymbol{H}, \boldsymbol{J}\right\}_{\mathbf{r},t} = \frac{1}{16\pi^4} \iiint_{\mathbb{R}^3} \mathrm{d}\boldsymbol{\kappa} \int_{-\infty}^{+\infty} \left\{\breve{\mathbf{E}}, \breve{\mathbf{H}}, \breve{\mathbf{J}}\right\}_{\boldsymbol{\kappa},\omega} e^{-i(\boldsymbol{\kappa}\cdot\mathbf{r}-\omega t)} \mathrm{d}\omega, \tag{11}$$

3 The Einstein convention on repeated indexes is used for brevity.

where $\boldsymbol{\kappa} = \kappa_m \hat{\mathbf{x}}^m$, from Eq. (9) we can obtain the following spectral-domain Maxwell equations:

$$-i\boldsymbol{\kappa} \times \left\{ \begin{array}{c} \breve{\mathbf{E}} \\ \breve{\mathbf{H}} \end{array} \right\}_{\boldsymbol{\kappa},\,\omega} = i\omega \left\{ \begin{array}{c} -\mu_0 \breve{\mathbf{H}} \\ \varepsilon_0 \breve{\mathbf{E}} \end{array} \right\}_{\boldsymbol{\kappa},\,\omega} + \left\{ \begin{array}{c} \mathbf{0} \\ \breve{\mathbf{J}} \end{array} \right\}_{\boldsymbol{\kappa},\,\omega}. \qquad (12)$$

The solution of Eq. (12) is merely algebraic [18]:

$$\left\{ \begin{array}{c} \breve{\mathbf{E}} \\ \breve{\mathbf{H}} \end{array} \right\}_{\boldsymbol{\kappa},\,\omega} = \frac{1}{\boldsymbol{\kappa}\cdot\boldsymbol{\kappa} - \omega^2 c^{-2}} \left\{ \begin{array}{c} -i\omega\mu_0 \left(\underline{\underline{I}} - \dfrac{\boldsymbol{\kappa}\otimes\boldsymbol{\kappa}}{\omega^2 c^{-2}} \right) \cdot \\ -i\boldsymbol{\kappa}\times \end{array} \right\} \breve{\mathbf{J}}(\boldsymbol{\kappa},\,\omega), \quad (13)$$

where $\underline{\underline{I}} = \delta_{l,\,m}\hat{\mathbf{x}}^l \otimes \hat{\mathbf{x}}^m$ ($\delta_{l,\,m}$ is the Kronecker symbol) and $c = 1/\sqrt{\varepsilon_0\mu_0}$ is the speed of light in vacuum.

By replacing Eq. (13) in the quadruple Fourier anti-transformation formula (11), it is possible to obtain a 'proper' EM PW spectral representation of the space-time domain fields $\{\boldsymbol{E},\,\boldsymbol{H}\}_{\mathbf{r},\,t}$ in terms of a triple integral expansion, provided that the integration with respect to one of the four spectral variables (e.g., κ_1) is performed through residual calculation at the polar singularities of the integrand, i.e., at $||\boldsymbol{\kappa}||^2 - \omega^2 c^{-2} = 0$: for instance, the integration with respect to the real variable κ_1 can be evaluated by means of a contour integration in the complex κ_1-plane, where the contour shall be composed of the real κ_1-axis and the infinite semicircle, through the upper half-plane (for $x_1 > 0$) or the lower half-plane (for $x_1 < 0$), with the last condition stated by the Jordan's lemma so that the semicircle integration shall vanish at the infinite radius limit; in this way the poles $\tilde{\kappa}_1 = \sqrt{\omega^2 c^{-2} - \tilde{\kappa}_2^2 - \tilde{\kappa}_3^2}$ (with $\operatorname{Im}\tilde{\kappa}_1 < 0$) or $-\tilde{\kappa}_1$ have to be considered for $x_1 > 0$ or $x_1 < 0$, respectively [20]. By evaluating the corresponding residuals we get:

$$\left\{ \begin{array}{c} \boldsymbol{E} \\ \boldsymbol{H} \end{array} \right\}_{\mathbf{r},\,t} = \frac{i}{8\pi^3} \iiint\limits_{\mathbb{R}^3} \left\{ \begin{array}{c} -i\omega\mu_0 \left(\underline{\underline{I}} - \dfrac{\tilde{\boldsymbol{\kappa}}_\pm \otimes \tilde{\boldsymbol{\kappa}}_\pm}{\omega^2 c^{-2}} \right) \cdot \\ -i\tilde{\boldsymbol{\kappa}}_\pm \times \end{array} \right\}$$
$$\times \frac{\breve{\mathbf{J}}(\tilde{\boldsymbol{\kappa}}_\pm,\,\omega)}{2\tilde{\kappa_1}} e^{-i(\tilde{\boldsymbol{\kappa}_\pm}\cdot\mathbf{r} - \omega t)} \mathrm{d}\kappa_2 \mathrm{d}\kappa_3 \mathrm{d}\omega, \qquad (14)$$

with:

$$\tilde{\boldsymbol{\kappa}}^{\pm} = \pm\tilde{\kappa_1}\hat{\mathbf{x}} + \tilde{\kappa_2}\hat{\mathbf{y}} + \tilde{\kappa_3}\hat{\mathbf{z}} = \pm\hat{\mathbf{x}}\sqrt{\omega^2 c^{-2} - \kappa_2^2 - \kappa_3^2} + \kappa_2\hat{\mathbf{y}} + \kappa_3\hat{\mathbf{z}}, \quad (15)$$

where upper and lower signs are valid for $x_1 > 0$ and $x_1 < 0$, respectively.

It is important to remark that each PW integrand term in Eq. (14) is an individual solution of the source-less Maxwell equation, i.e., verifies Eq. (19) for $\boldsymbol{J} \equiv \boldsymbol{0}$; in such sense this triple-integral formula represents a 'proper' EM PW expansion.

3.2. Generalization to the Special Relativistic Case

At the outset we distinguish two reference frames: Σ, where the antenna appears at rest, and Σ', where the receiver is at rest. The relative translation velocity of the antenna with respect to the receiver is assumed to be $\beta c \hat{\mathbf{x}}^3$.

As a first step of the FHM, by starting from the knowledge of the source current distribution $\boldsymbol{J}(\mathbf{r}, t)$ as measured by an observer at rest with respect to the antenna we can solve the radiation problem in the co-moving frame Σ on the ground of the approach depicted in the previous section, obtaining the EM PW triple integral expansion given by Eq. (14), that can be recast as follows (let $\zeta = \sqrt{\mu_0/\varepsilon_0}$):

$$\left\{ \begin{array}{c} \boldsymbol{E} \\ \boldsymbol{H} \end{array} \right\}_{\mathbf{r},\, t} = \frac{i}{8\pi^3} \iiint\limits_{\mathbb{R}^3} \frac{e^{-i\omega c^{-1}(\hat{\boldsymbol{\kappa}}_\pm \cdot \mathbf{r} - ct)}}{2\hat{\kappa}_1} \left\{ \begin{array}{c} \zeta \underline{\underline{\Psi}}_{\mathrm{E}} \\ \underline{\underline{\Psi}}_{\mathrm{H}} \end{array} \right\}_{\hat{\boldsymbol{\kappa}}_\pm} \cdot \breve{\mathbf{J}}(\tilde{\boldsymbol{\kappa}}_\pm, \omega) \mathrm{d}\kappa_2 \mathrm{d}\kappa_3 \mathrm{d}\omega, \tag{16}$$

where we defined the PW propagation unit-vector $\hat{\boldsymbol{\kappa}}_\pm$, i.e.:

$$\hat{\boldsymbol{\kappa}}_\pm = \omega^{-1} c \tilde{\boldsymbol{\kappa}}_\pm = \pm \hat{\kappa}_1 \hat{\mathbf{x}}^1 + \hat{\kappa_2} \hat{\mathbf{x}}^2 + \hat{\kappa_3} \hat{\mathbf{x}}^3;$$

$$\hat{\kappa}_m = \omega^{-1} c \kappa_m, \quad m = 2,\, 3; \qquad \hat{\kappa}_1 = \sqrt{1 - \hat{\kappa}_2^2 - \hat{\kappa}_3^2}; \tag{17}$$

the "PW vector orientation tensors" $\{\underline{\underline{\Psi}}_E, \underline{\underline{\Psi}}_H\}_{\hat{\boldsymbol{\kappa}}_\pm}$ define the orientation of the various vector components of every spectral term occurring in the PW integral expansion; in general for a non-specific PW propagation unit-vector $\hat{\mathbf{k}} = \hat{\mathbf{x}}^m \hat{k}_m (\hat{\mathbf{k}} \cdot \hat{\mathbf{k}} = \hat{k}_m \hat{k}_n \delta_{m,\,n} = 1)$ they have the following expression[4]:

$$\left\{ \underline{\underline{\Psi}}_{\mathrm{E}}, \underline{\underline{\Psi}}_{\mathrm{H}} \right\}_{\hat{\mathbf{k}}} = \left\{ \left(\delta_{l,\,m} - \hat{k}_l \hat{k}_m \right) \hat{\mathbf{x}}^l \otimes \hat{\mathbf{x}}^m,\, \varepsilon_{l,\,s,\,m} \hat{k}_s \hat{\mathbf{x}}^l \otimes \hat{\mathbf{x}}^m \right\}. \tag{18}$$

Then, as second step of the FHM, the $\Sigma \to \Sigma'$ FRCT shall be applied to the EM PW spectral expansion given by Eq. (16) in order to obtain the expression of the EM fields $\{\boldsymbol{E}', \boldsymbol{H}'\}$ as experienced by a receiver at rest in frame Σ' at position $\mathbf{r}' = x'_m \hat{\mathbf{x}}^m$ and time t', where

4 $\varepsilon_{l,s,m}$ is Levi-Civita symbol, i.e., it is equal to $+1$ or -1 if $\{l,\, s,\, m\}$ is an even or an odd permutation of $\{1,\, 2,\, 3\}$, respectively; otherwise it is equal to 0.

according to the $\Sigma \leftrightarrow \Sigma'$ Lorentz coordinate transformations we have (let $\gamma = +\sqrt{1-\beta^2}$):

$$x'_m = x_m, \quad m = 1,2; \quad x'_3 = \gamma(x_3 + \beta ct); \quad t' = \gamma(t + \beta c^{-1} x_3). \tag{19}$$

When the EM field is expressed in terms of a superposition of elementary terms the intrinsic linear nature of the FRCT can be exploited; moreover, in the case of EM PW expansion given by Eq. (16) each elementary term has individual relativistic covariance properties since it is a special solution of the source-less Maxwell equations. Therefore the $\Sigma \leftrightarrow \Sigma'$ FRCT of the PW integral summation shall be expressed as the integral summation of the various $\Sigma \leftrightarrow \Sigma'$ covariance-transformed plane waves.

It is well-known that the analytic action of the FRCT on PWs can expressed through simple parameters alteration rules [10–13, 21]. In particular, the application of the $\Sigma \leftrightarrow \Sigma'$ FRCT to a given PW term modifies its angular frequency ω and its unit PW-vector $\hat{\boldsymbol{\kappa}}_{\pm}$ as follows:

$$\omega \rightarrow \omega' = \gamma(1 + \beta\hat{\kappa}_3)\omega \tag{20}$$

$$\begin{aligned} \hat{\boldsymbol{\kappa}}_{\pm} \rightarrow \hat{\boldsymbol{\kappa}}'_{\pm} &= \pm\hat{\kappa}'_1\hat{\mathbf{x}}^1 + \hat{\kappa}'_2\hat{\mathbf{x}}^2 + \hat{\kappa}'_3\hat{\mathbf{x}}^3 \\ &= \frac{\pm\gamma^{-1}\hat{\kappa}_1\hat{\mathbf{x}}^1 + \gamma^{-1}\hat{\kappa}_2\hat{\mathbf{x}}^2 + (\hat{\kappa}_3 + \beta)\hat{\mathbf{x}}^3}{1 + \beta\hat{\kappa}_3}. \end{aligned} \tag{21}$$

Eqs. (20) and (21) take into account the Doppler frequency shift and the zenithal aberration, respectively. When covariance-transforming PW terms in Eq. (16), the Doppler frequency shift $\omega \rightarrow \omega'$ has to be taken into account in the exponential phase term, whilst the zenithal aberration, consequent to the $\hat{\boldsymbol{\kappa}}_{\pm} \rightarrow \hat{\boldsymbol{\kappa}}'_{\pm}$ variation, has to be taken into account both in the phase term and in the PW orientation tensors [17].

On the other hand, the FRCT does not alter the shape of the polarization ellipse of the given PW term (Stokes parameters are special-relativistic invariants [21]), but only produces an isotropic amplitude expansion according to the factor $\gamma(1 + \beta\hat{\kappa}_3)$ [17].

By exploiting the aforementioned results, the following EM PW expansion of radiated fields in the observer rest frame Σ' can be obtained:

$$\begin{aligned} \left\{ \begin{array}{c} \boldsymbol{E}' \\ \boldsymbol{H}' \end{array} \right\}_{\mathbf{r}',\, t'} = \frac{i}{8\pi^3} \iiint\limits_{\kappa_2,\, \kappa_3,\, \omega \in \mathbb{R}^3} \frac{\gamma(1 + \beta\hat{\kappa}_3)}{2\hat{\kappa}_1} e^{-i\omega' c^{-1}(\hat{\boldsymbol{\kappa}}'_{\pm} \cdot \mathbf{r}' - ct')} \\ \times \left\{ \begin{array}{c} \zeta \underline{\underline{\Psi}}_{\mathrm{E}} \\ \underline{\underline{\Psi}}_{\mathrm{H}} \end{array} \right\}_{\hat{\boldsymbol{\kappa}}'_{\pm}} \cdot \breve{\mathbf{J}}(\tilde{\boldsymbol{\kappa}}_{\pm}, \omega) \mathrm{d}\kappa_2 \mathrm{d}\kappa_3 \mathrm{d}\omega, \end{aligned} \tag{22}$$

with upper and lower signs valid for $x'_1 > 0$ and $x'_1 < 0$, respectively.

3.3. Doppler Spectra

As one can see from Eq. (22), the Doppler effect phenomenon involves that in frame Σ' the PW expansion of the radiated field is always multi-chromatic, even in the particular case of a mono-chromatic source current distribution (i.e., if $\breve{\mathbf{J}}(\boldsymbol{\kappa}, \omega) = \breve{\mathbf{j}}(\boldsymbol{\kappa})\delta(\omega - \omega_0)$, for $\omega > 0$); in the case of point, according to Eqs. (20) and (17) a PW spectral component relevant to a specific value of the independent spectral triplet $\{\kappa_2, \kappa_3, \omega\}$ is characterized by the following value of the angular frequency:

$$\omega' = \gamma(\omega + \beta c \kappa_3). \tag{23}$$

In fact, the EM field expansion (22) can be recast as follows:

$$\left\{ \begin{array}{c} \boldsymbol{E}' \\ \boldsymbol{H}' \end{array} \right\}_{\mathbf{r}', t'} = \frac{i}{8\pi^3} \iiint\limits_{\kappa_2, \kappa_3, \omega \in \mathbb{R}^3} \left\{ \begin{array}{c} \boldsymbol{\eta}'_{\mathrm{E}} \\ \boldsymbol{\eta}'_{\mathrm{H}} \end{array} \right\}_{\mathbf{r}'; \kappa_2, \kappa_3, \omega} e^{i\gamma(\omega + \beta c \kappa_3)t'} \mathrm{d}\kappa_2 \mathrm{d}\kappa_3 \mathrm{d}\omega, \tag{24}$$

with:

$$\left\{ \begin{array}{c} \boldsymbol{\eta}'_{\mathrm{E}} \\ \boldsymbol{\eta}'_{\mathrm{H}} \end{array} \right\}_{\mathbf{r}'; \kappa_2, \kappa_3, \omega} = \frac{i}{8\pi^3} \frac{\gamma(1 + \beta\hat{\kappa}_3)}{2\hat{\kappa}_1} e^{-i\omega' c^{-1} \hat{\boldsymbol{\kappa}}'_{\pm} \cdot \mathbf{r}'} \left\{ \begin{array}{c} \zeta \underline{\underline{\Psi}}_{\mathrm{E}} \\ \underline{\underline{\Psi}}_{\mathrm{H}} \end{array} \right\}_{\mathbf{r}'; \kappa_2, \kappa_3, \omega} \cdot \breve{\mathbf{J}}(\tilde{\boldsymbol{\kappa}}_{\pm}, \omega), \tag{25}$$

where parameters $\hat{\boldsymbol{\kappa}}'_{\pm}$, $\hat{\kappa}_1$, $\hat{\kappa}_3$, $\tilde{\boldsymbol{\kappa}}_{\pm}$ are related to the independent spectral variables κ_2, κ_3, ω according to Eqs. (15), (17) and (21).

Long-term measurements by a spectrum analyser located at a given fixed position $\mathbf{r}'$ in frame Σ' can be represented by means of the Fourier frequency transform to the variable Ω', i.e.:

$$\left\{ \begin{array}{c} \mathbf{e}' \\ \mathbf{h}' \end{array} \right\}_{\mathbf{r}', \Omega'} = \int\limits_{-\infty}^{+\infty} \left\{ \begin{array}{c} \boldsymbol{E}' \\ \boldsymbol{H}' \end{array} \right\}_{\mathbf{r}', t'} e^{-i\Omega' t'} \mathrm{d}t', \tag{26}$$

where Ω' is the observation frequency. Such transform (hereinafter named *Doppler frequency spectrum*) can be evaluated starting from Eq. (24) in the following closed-form by exploiting some properties of the Dirac-δ distribution (see Refs. [13, 21]):

$$\left\{ \begin{array}{c} \mathbf{e}' \\ \mathbf{h}' \end{array} \right\}_{\mathbf{r}', \Omega'} = \frac{1}{\gamma\beta c} \iint\limits_{\kappa_2, \omega \in \mathbb{R}^2} \left\{ \begin{array}{c} \boldsymbol{\eta}'_{\mathrm{E}} \\ \boldsymbol{\eta}'_{\mathrm{H}} \end{array} \right\}_{\mathbf{r}'; \kappa_2, \overline{\kappa}_3, \omega} \mathrm{d}\kappa_2 \mathrm{d}\omega, \tag{27}$$

with:

$$\overline{\kappa}_3 = \beta^{-1}c^{-1}(\gamma^{-1}\Omega' - \omega). \tag{28}$$

3.4. The Sierpinski Carpet Antenna

As an application we consider the specific case of a moving planar antenna, whose 2-dimensional electric current pattern is the N^{th} order pre-fractal of the Sierpinski carpet, i.e., (in the antenna rest frame Σ):

$$\boldsymbol{J}(\mathbf{r},\, t) = J\hat{\boldsymbol{\alpha}}\chi_{\check{S}_{2,\,N}}\left\{\frac{x_1}{\Delta},\, \frac{x_3}{\Delta}\right\}\delta(x_2)\cos\omega_0 t, \tag{29}$$

We assume, for simplicity[5], that on every element of the carpet — which lies on plane $x_2 = 0$ and has width Δ — the electric current density has constant amplitude J and orientation along the $\hat{\boldsymbol{\alpha}} = \hat{\mathbf{x}}^1\cos\alpha + \hat{\mathbf{x}}^3\sin\alpha$ axis, and that the feeding signal is purely monochromatic with wave-length λ (angular frequency $\omega_0 = 2\pi c/\lambda$). Thus the spectral transform of the current distribution, that is needed for evaluating the radiated EM field through to the above-mentioned PW technique, reads as follows:

$$\breve{\mathbf{J}}(\boldsymbol{\kappa},\, \omega) = J\hat{\boldsymbol{\alpha}}\Delta^2\breve{\chi}_{\check{S}_{2,\,N}}(\kappa_1\Delta,\, \kappa_3\Delta)\delta(\omega - \omega_0) \tag{30}$$

Then, an extensive numerical analysis of the Doppler spectra (relevant to the Poynting vector $\frac{1}{2}\mathbf{e}' \times \mathbf{h}'$) was performed by varying all the involved geometrical parameters[6]. The results show that the bandwidth $\mathrm{d}\Omega'$ of the received signal depends only on β ($\mathrm{d}\,\Omega' \sim 2\beta\omega_0$) for low values of β); whereas the shape of the spectrum is mainly dependent on the carpet width/wavelength ratio $\delta = \Delta/\lambda$ and on the pre-fractal order N. In the case of point, for low values of δ (approximately $\delta < 1$) Doppler spectra present an elementary shape spread around the 'nominal' frequency ω_0, with the presence of only two principal peaks, corresponding to a 'red-shifted' ($\Omega' < \omega_0$) and a 'blue-shifted' ($\Omega' > \omega_0$) *Doppler-tunes* (see Fig. 3, left); this happens for any value of N. On the other hand, for higher values of δ the shape of the spectra gets more and more complex, with the presence

5 More general orientations of the antenna can be straightforwardly considered by introducing auxiliary rotated coordinate system. Also, the additional presence of a reflecting plane substrate can be taken into account by considering the reflection of the free-space term given by Eq. (16) (static case) or Eq. (22) (relativistic case) on the ground of Snell and Fresnell laws, see [13, 21].

6 By virtue of the similitude theorem, for a given choice of the observation point $\mathbf{r}' = \lambda \cdot \xi'_m\hat{\mathbf{x}}^m$ and of the carpet width $\Delta = \delta\lambda$, results are a-priori independent of the value of the wave-length λ. Also, by symmetry, Doppler spectra (26) evaluated on an infinite time-window must be independent of coordinate $x'_3 = \mathbf{r}' \cdot \hat{\mathbf{x}}^3$.

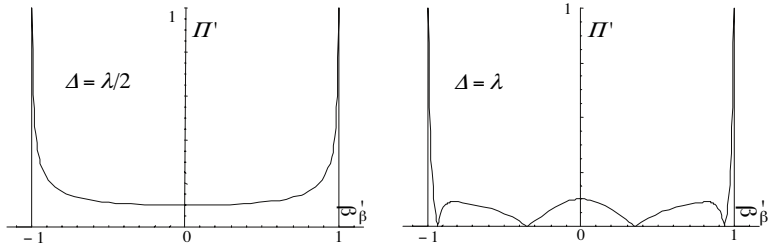

Figure 3. Normalized spectral amplitude of the Poynting vector $\Pi'(\Omega') = P'(\Omega')/\max P'(\omega')$, $P'(\Omega') = ||\frac{1}{2}\mathbf{e}'(\mathbf{r}', \Omega') \times \mathbf{h}'(\mathbf{r}', \Omega')||$ vs. normalized frequency shift $\varpi'_\beta = (\Omega'/\omega_0 - 1)/\beta$ at fixed position $\mathbf{r}' = \lambda(4\hat{\mathbf{x}}^1 + 3\hat{\mathbf{x}}^2)$; relative velocity $\beta = 10^{-6}$; $\alpha = \pi/4$; carpet width $\Delta = \delta\lambda$, width $\delta = 0.5$ (left) and $\delta = 1$ (right); pre-factal order $N = 3$.

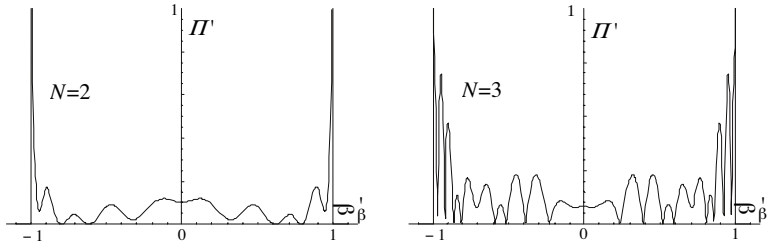

Figure 4. The same as Fig. 3 except $\delta = 5$, with pre-fractal order $N = 2$ (left) and $N = 3$ (right).

of various in-band secondary peaks and minima; *ceteris paribus*, the shape is more complex for higher order N (see Fig. 3, right, and Fig. 4).

For low values of β Doppler spectra appear to be symmetrical with respect to ω_0; on the other hand, asymmetry phenomena arise for relativistic speeds, i.e for $\beta \to 1$, with $\mathrm{d}\Omega'$ that gets larger than $2\beta\omega_0$ (see Fig. 5); such result is consistent with analogous data present in the literature relevant to EM radiators and scatterers moving at speeds close to the light velocity [13, 21].

3.5. Instantaneous Modulations

Doppler spectra furnish a description relevant to long-term signal measurements (i.e., for an observation time-window $\tau' \gg \omega_0^{-1}$) on the EM field radiated by a moving antenna; on the other hand, for short-term observations the signal associated to a generic scalar component

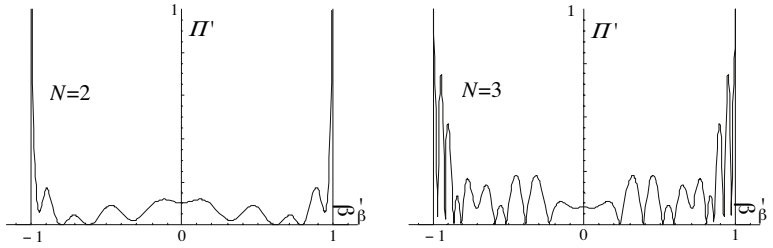

Figure 5. The same as Fig. 4 except $\beta = 0.3$, with pre-fractal order $N = 2$ (left) and $N = 3$ (right).

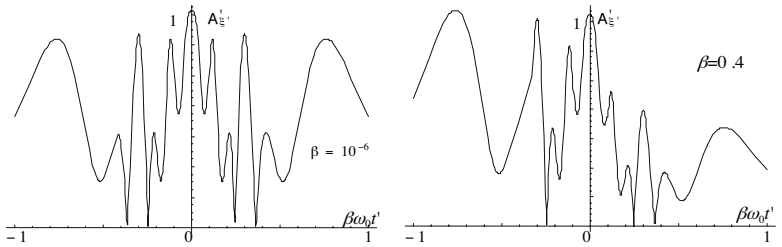

Figure 6. Normalized instantaneous amplitude modulation $A'_{\xi'}(t') = a'_{\xi'}(t')/a'_{\xi'}(0)$, relevant to the signal $\xi'(t') = \boldsymbol{H}'(\mathbf{r}', t')\cdot\hat{\mathbf{x}}^3$ vs. normalized time $\beta\omega_0 t'$, for $\beta = 10^{-6}$ (left) and $\beta = 0.4$ (right); fixed observer located at position $\mathbf{r}' = 5\lambda\hat{\mathbf{x}}^2$; carpet parameters: $\alpha = 0$, $\Delta = 3\lambda$, $N = 3$.

ξ' of the EM field experienced at a fixed position $\mathbf{r}'$, whose expression is given by Eq. (22), presents instantaneous amplitude modulation $a'_{\xi'}$ and frequency modulation $\nu'_{\xi'}$; they correspond to the amplitude $|\Xi'|$ and to the argument sign-reversal time-derivative $-\partial \mathrm{Arg}\Xi'/\partial t'$ of the complex modulation (with respect to the nominal frequency ω_0) Ξ', respectively, i.e.,[7] [22]:

$$\Xi(t';\,\omega_0) \equiv \mathrm{Re}\Xi'(t') + i\mathrm{Im}\Xi'(t');$$

$$\begin{pmatrix} \mathrm{Re}\Xi'(t') \\ \mathrm{Im}\Xi'(t') \end{pmatrix} = \begin{pmatrix} \cos\omega_0 t' & \sin\omega_0 t' \\ -\sin\omega_o t' & \cos\omega_0 t' \end{pmatrix} \begin{pmatrix} \xi'(t') \\ \xi'(t') \circledast \frac{1}{\pi t'} \end{pmatrix}, \qquad (31)$$

As it can be seen in Fig. 6, the variation of the instantaneous amplitude with time t' is monotonic when the distance $||\mathbf{r}' - \beta ct'\hat{\mathbf{x}}^3||$ between the

7 Symbol '$\circledast$' represents the convolution product computed as Cauchy's principal value.

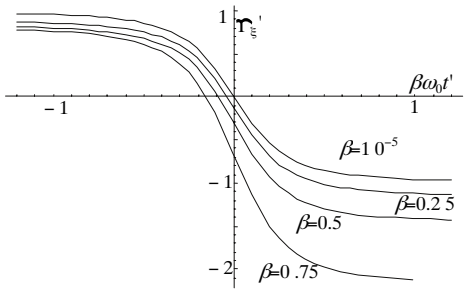

Figure 7. Normalized frequency shift $\Upsilon'_{\xi'} = (\nu'_{\xi'}/\omega_0 - 1)/\beta$, relevant to various values of β, for the same conditions of Fig. 6.

antenna and the observer is great (quasi-stationary far-field condition), whilst, as the distance goes to the minimum, i.e., for $t' \to 0$, the signal rapidly oscillates between maximum and minimum levels (non-stationary near-field condition); a peculiar relativistic effect is that at high velocities the symmetry between the amplitude values at opposite instants t' and $-t'$ (when the distances between antenna and observer are the same) is lost, see [13]. An analogous high-velocity asymmetry affects the frequency shift diagrams: as one can see in Fig. 7, negative ('red') shift is present at some time interval $t' < 0$, when the antenna is still approaching the observer and then positive ('blue') shift would be expected according to the non-relativistic theory, see [13, 23]; moreover steady-state blue ($t' \to +\infty$) and red ($t' \to -\infty$) shifts assume non-symmetric values[8].

3.6. Far-field Properties

The PW spectrum given by Eq. (16), valid for observers in the antenna rest frame Σ, is compound by waves of the uniform type and of the non-uniform evanescent type for $\hat{\kappa}_2^2 + \hat{\kappa}_3^2 \leq 1$ and $\hat{\kappa}_2^2 + \hat{\kappa}_3^2 > 1$, respectively. In the far-field[9] the last ones give negligible contributes to the integral expansion and thus the sum can be restricted to the only PW terms whose propagation unit vector $\hat{\boldsymbol{\kappa}}$ is real, i.e.:

$$\hat{\boldsymbol{\kappa}} = \hat{\mathbf{x}}^m \hat{\kappa}_m = \hat{\mathbf{x}}^1 \sin\theta\cos\phi + \hat{\mathbf{x}}^2 \sin\theta\sin\phi + \hat{\mathbf{x}}^3 \cos\theta,$$

$$(\theta,\, \phi) \in [0,\, \pi] \times [-\pi,\, \pi[. \tag{32}$$

8 Instead $\lim_{t' \to \pm\infty} \Upsilon'_{\xi'}(t') \approx \mp 1$ for low values of β.

9 i.e., for $x_1 = x'_1 \gg \lambda = 2\pi c/\omega_0$ in the specific monochromatic case under exam.

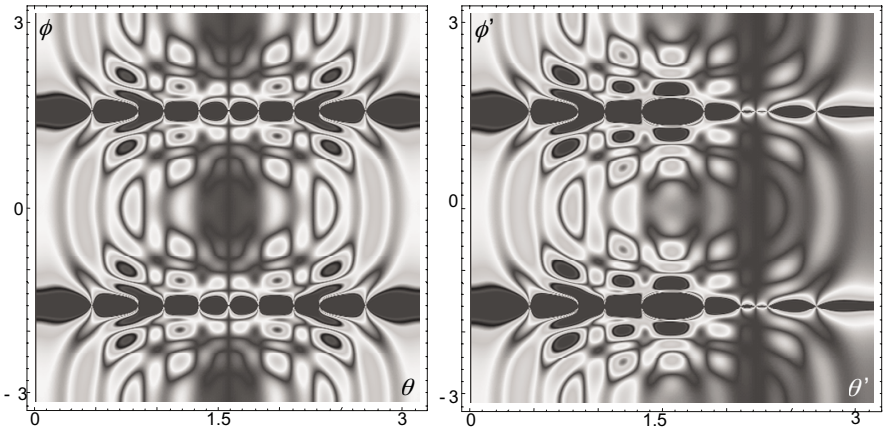

Figure 8. Chromatic plots of the far-field normalized radiation patterns (relevant to the Poynting vector) in terms of polar angles. Carpet parameters: $\alpha = \pi/2$, $\Delta = 4\lambda$, $N = 3$. Left: motionless case. Right: relativistic case for $\beta = 0.6$.

Thus, once recast the integral expansion (16) in terms of the independent polar variables θ and ϕ the far-field radiation patterns can be immediately obtained from the inspection of the amplitude of the various PW terms. As it can be seen in Fig. 8 (left), the radiation pattern relevant to the Sierpinski carpet-like current source given by Eq. (29) exhibits zenithal and azimuthal symmetries with respect to values $\theta = \pi/2$ and $\phi = 0$, respectively.

The aforementioned approach for evaluating far field diagrams can be extended to the relativistic case; in fact, from Eq. (21) it is straightforward to show that a PW, which appears to be uniform in frame Σ with real PW unit vector $\hat{\boldsymbol{\kappa}}$ given by Eq. (32), still appears to be uniform as seen in frame Σ', and its PW unit vector becomes [13, 21]:

$$\hat{\boldsymbol{\kappa}}' = \hat{\mathbf{x}}^m \hat{\kappa}'_m = \hat{\mathbf{x}}^1 \sin\theta' \cos\phi' + \hat{\mathbf{x}}^2 \sin\theta' \sin\phi' + \hat{\mathbf{x}}^3 \cos\theta' \quad (33)$$

$$\cos\theta' = \frac{\cos\theta}{1 + \beta\cos\theta}, \quad \sin\theta' = \frac{\sin\theta}{\gamma(1 + \beta\cos\theta)}, \quad \phi' = \phi, \quad (34)$$

Therefore, by taking into account Eqs. (32), (33), (34) the integral expression in Eq. (22) can be recast in terms of the new couple of independent polar variables θ' and ϕ' and then far-field radiation patters can be obtained. Since the antenna appears in motion in frame Σ', it is important to point out that such patterns have to be understood as "instantaneous" ones [13]: in the case of point, they shall

represent an instantaneous 'photograph' of the far-field distribution as it could be virtually taken at time t' by a fixed observer that would be located at the current position of the center of the translating antenna, i.e., at $\beta ct'\hat{\mathbf{x}}^3$ (i.e., the point $\beta ct'\hat{\mathbf{x}}^3$ shall act as "instantaneous" pole of the angular reference system). From numerical analysis it appears that for low velocities the shape of the normalized radiation diagrams remains substantially unaltered with respect to the motionless case. Whereas, as β is taken toward the relativistic limit $\beta \to 1$ (practically for $\beta > 0.1$), the pattern becomes more and more asymmetric with respect to the zenithal angle $\theta' = \pi/2$ (see Fig. 8, right); on the other hand no asymmetry is experienced for the azimuth[10]. The detection of such high-speed phenomenon for the fractal antenna under exam is coherent with data relevant to far-field properties of elementary radiators in motion at velocity close to the relativistic limit [13].

4. CONCLUSIONS

This work presents a PW spectral approach to the study of EM (pre-)fractal radiators: on the ground of an efficient iterative procedure for the description of the source current distribution in the Fourier-domain it can furnish closed-form solutions for the wide-ranging class of geometries whose generating IFS is based on affinities. The integral PW representation allows us a straightforward generalization to the relativistic case, that is important in order to outline a theoretical framework for the project of fractal radiators for mobile systems. The example of a planar Sierpinski carpet antenna is studied in details, providing analytical and numerical results on Doppler spectra, instantaneous modulations and far-field radiation patterns.

ACKNOWLEDGMENT

This work was financially supported by the European Commission through FET project IST-2001-33055

APPENDIX A. ITERATED FUNCTION SYSTEMS

Let (S, d) a metric space. An *Iterated Function System* (IFS) in S is a set of p different contraction mappings, $\{w_1, w_2, \ldots, w_p\}$, with $w_j : S \to S$ and contraction ratios $c_1, c_2, \ldots, c_p \in [0, 1[$, $1 \leq j \leq p$, such that $\mathrm{d}(w_j(x), w_j(y)) \leq c_j \mathrm{d}(x, y)$, $\forall x, y \in S$. It can be shown

10 In fact the relativistic transformation (34) involves a zenithal aberration but no azimuthal aberration.

that if $\wp_{\copyright}(S)$ is the set of all the compact subsets of S, $\wp_{\copyright}(S)$ is a complete metric space with respect to the Hausdorff metric induced from (S, d), and map $w : \wp_{\copyright}(S) \to \wp_{\copyright}(S)$ defined as follows

$$\wp_{\copyright}(E) \ni E \mapsto w(E) := \bigcup_{j=1}^{p} w_j(E), \tag{A1}$$

is a contraction and thus admits one fixed-point $E_\infty \in \wp_{\copyright}(S)$, (which is also called 'attractor' of the IFS as a subset $E_\infty \subset S$) [18]. Formally, this means that:

$$E_\infty = \lim_n w^n(E) = \bigcap_{n=0}^{\infty} w^n(E). \tag{A2}$$

Here w^n means the composition of w with itself n times, i.e., the n^{th} iterate of w; $w^n(E)$ is also called the N^{th} prefractal of the given IFS (and of initiator E). Attractors of IFSs often show self-similarity properties, i.e., they are made up of similar copies of themselves at infinitely smaller and smaller length-scales. This is one of the main features of 'fractal' sets, which is quantitatively represented by their non-integer fractal dimensions. One of these, the *Hausdorff dimension* $\dim_{\mathrm{H}} E_\infty$, in the case of 'just-touching' IFSs (i.e., when $w_i(E)^\circ \cap w_j(E)^\circ = \oslash$, $1 \le i \le j \le p$), is given by the solution of the following equation:

$$\sum_{j=1}^{p} c_j^{\dim_{\mathrm{H}} E_\infty} = 1. \tag{A3}$$

For more details on self-similarity, IFSs and fractal dimensions, cfr. [18, 19].

REFERENCES

1. Werner, D. H. and R. Mittra (eds.), *Frontiers in Electromagnetics*, Chps. 1–3, IEEE Press, Piscataway, NJ, 2000.
2. Jaggard, D. L. and X. Sun, "Reflection from fractal layers," *Opt. Lett.*, Vol. 15, No. 24, 1428–1430, Dec. 1990.
3. Walker, J. G. and J. R. James, "Fractal volume antennas," *Electron. Lett.*, Vol. 28, No. 11, 1536–1537, Nov. 1998.
4. Puente-Baliarda, C. and R. Pous, "Fractal design of multiband and low side-lobe arrays," *IEEE Trans. Antennas Propagat.*, Vol. 44, No. 5, 1–10, May 1996.

5. Puente-Baliarda, C., J. Romeu, R. Pous, and A. Cardama, "On the behaviour of the Sierpinski multiband fractal antenna," *IEEE Trans. Antennas Propagat.*, Vol. 46, No. 4, 517–524, Apr. 1998.
6. Best, S. R., "On the significance of self-similar fractal geometry in determining the multi-band behaviour of the Sierpinski gasket antenna," *IEEE Antennas Wirel. Propagat. Lett.*, Vol. 1, 22–25, 2002.
7. Arrighetti, W. and G. Gerosa, "Spectral analysis of Šerpisnkij carpet-like prefractal waveguides and resonators," *IEEE Microw. Wirel. Co. Lett.*, Vol. 15, No. 1, 30–32, Jan. 2005.
8. Arrighetti, W. and G. Gerosa, "Can you hear the fractal dimension of a drum?" *Applied and Industrial Mathematics in Italy*, M. Primicerio, R. Spigler, and V. Valente (eds.), 65–75, World Scientific, 2005.
9. Giona, M., "Contour integrals and vector calculus on fractal curves and interfaces," *Chaos Solitons and Fractals*, Vol. 10, No. 8, 1349–1370, Aug. 1999.
10. Van Bladel, J., *Relativity and Engineering*, Springer-Verlag, New York, 1984.
11. De Zutter, D., "Green's functions for the Fourier spectra of the field form two-dimensional sources or scatterers in uniform motion," *Radio Sci.*, Vol. 22, No. 7, 1197–1203, Dec. 1987.
12. Censor, D., "Scattering in velocity dependent systems," *Radio Sci.*, Vol. 7, No. 2, 331–337, Feb. 1972.
13. De Cupis, P., "Radiation by a moving wire-antenna in the presence of interface," *JEMWA*, Vol. 14, No. 8, 1197–1203, Aug. 2000.
14. Censor, D., "The mathematical elements of relativistic free-space scattering," *JEMWA*, Vol. 19, 907–923, 2005.
15. Censor, D., "Free-space multiple scattering by moving objects," *JEMWA*, Vol. 19, 1157–1170, 2005.
16. Censor, D., I. Arnaoudov, and G. Venkov, "Differential-operators for and elliptical wave-functions in free-space relativistic scattering," *JEMWA*, Vol. 19, 1251–1266, 2005.
17. De Cupis, P., G. Gerosa, and G. Schettini, "Electromagnetic scattering by uniformly moving bodies," *JEMWA*, Vol. 14, No. 8, 1037–1062, Aug. 2000.
18. Barnsley, M. F., *Fractals Everywhere*, Academic Press, San Diego, 1988.
19. Falconer, K., *Fractal Geometry: Mathematical Foundations and Applications*, Wiley, NY, 1990.

20. De Hoop, A. T., *Handbook of Radiation and Scattering of Waves*, Academic Press, London, 1995.
21. De Cupis, P., "A relativistic theory of partially-polarized waves," *SIMAI 2002 Congress*, abstract 382, Chia Laguna, May 27–31, 2002.
22. Oppenheim, A. V. and P. W. Schaefer, *Digital Signal Processing*, Prentice-Hall, New Jersey, 1975.
23. Ben-Shimol, Y. and D. Censor, "Contribution to the problem of near-zone inverse doppler effect," *Radio Sci.*, Vol. 33, 463–474, 1998.